POLITECNICO
MILANO 1863

SCUOLA DI INGEGNERIA INDUSTRIALE
E DELL'INFORMAZIONE

Attitude Dynamics and Control for a 6U CubeSat

Authors:

ID	Surname	Name
10761243	Janus	Nemanja
10760901	Epaminonda	Athos
10620335	Picozzi	Riccardo
10620170	Scimone	Dario

Professor: Bernelli Zazzera Franco
Course: Spacecraft Attitude Dynamics
Academic Year: 2021-2022

Abstract

This report aims to model the attitude and control system of a 6U CubeSat; the simulations have been carried out inside the `Matlab&Simulink` environment. The satellite has been placed on sun-synchronous orbit; after modeling the environmental disturbances, the team studied the following three mission scenarios:

- *De-tumbling*: reduction of angular velocity after spacecraft deployment.
- *Pointing*: the spacecraft performs a slew maneuver to reach the desired direction.
- *Tracking*: the spacecraft maintains a specified attitude for all duration of the mission.

The results are presented via plot and simulation data analysis.

Keywords: Attitude Determination, Mission Analysis, CubeSat

Contents

List of Figures

List of Tables

List of Symbols

Variable	Description	Unit
$\boldsymbol{a}$	Semi-major axis of the orbit	km
$\underline{\boldsymbol{a}}_{J_2}$	Acceleration due to J2 perturbation	km/s^2
$\boldsymbol{\alpha_i}$	Weight coefficient of Wabha problem	–
$\underline{\boldsymbol{\alpha}}_d$	Desired orientation angles	$\circ$
$\boldsymbol{\alpha_x}$	Small rotation angle to model rotation error matrix	$\circ$
$\boldsymbol{\alpha_y}$	Small rotation angle to model rotation error matrix	$\circ$
$\boldsymbol{\alpha_z}$	Small rotation angle to model rotation error matrix	$\circ$
$\boldsymbol{A_d}$	Desired attitude matrix	–
$\boldsymbol{A_e}$	Error attitude matrix	–
$\boldsymbol{A_\epsilon}$	Direction cosine error matrix	–
$\boldsymbol{A_i}$	i-surface of the S/C	m^2
$\boldsymbol{A_{312}}$	Direction cosine rotation matrix with sequence 312	–
$\boldsymbol{A_{313}}$	Direction cosine rotation matrix with sequence 313	–
$\boldsymbol{A_{B/L}}$	Matrix of relative attitude between the body Frame and the LVLH	–
$\boldsymbol{A_{B/N}}$	Rotation matrix between inertial and body frame	–
$\boldsymbol{A_{L/N}}$	Matrix of relative attitude between the LVLH and inertial frame	–
$\dot{\underline{\boldsymbol{b}}}$	Rate random walk	rad/s^2
$\boldsymbol{b_N}$	Magnetic field in the inertial frame	T
$\boldsymbol{b_B}$	Magnetic field in the body frame	T
$\boldsymbol{e}$	Eccentricity of the orbit	–
$\boldsymbol{\epsilon}$	Obliquity angle between ecliptic and Earth's equator	$\circ$
$\boldsymbol{F_e}$	Total radiation on the S/C	W/m^2
$\boldsymbol{F_i}$	Force due to SRP on the i-surface	N
$\boldsymbol{g_n^m}$	Gaussian coefficient	nT
$\boldsymbol{h_n^m}$	Gaussian coefficient	nT
$\boldsymbol{H_0}$	Magnetic field evaluated at the first harmonic expansion	T
$\underline{\boldsymbol{h_r}}$	Reaction wheel angular momentum	rad/s^2
$\dot{\underline{\boldsymbol{h_r}}}$	Reaction wheel torque	rad/s^2

Variable	Description	Unit
$\boldsymbol{i}$	Inclination of the orbit	$\circ$
$\hat{\boldsymbol{i}}$	Direction of x axis in ECEI frame	$-$
$\underline{\underline{\boldsymbol{I}}}$	S/C Inertia matrix	$kg\ m^2$
$\hat{\boldsymbol{j}}$	Direction of x axis in ECEI frame	$-$
$\boldsymbol{J}$	Wabha problem function	$-$
$\boldsymbol{J_m}$	Minimum principal moment of inertia	$kg\ m^2$
$\boldsymbol{J_2}$	Perturbation value due to Earth's oblateness	$-$
$\boldsymbol{k}$	Scalar gain in Detumbling control logic	$-$
$\boldsymbol{\Lambda}$	Reaction wheels matrix	$-$
$\boldsymbol{\Lambda^*}$	Pseudoinvers reaction wheels matrix	$-$
$\underline{\hat{\boldsymbol{m}}}$	Magnetic dipole direction	$-$
$\underline{\boldsymbol{M}}$	Torques vector of Euler's equations	$N\ m$
$\underline{\boldsymbol{M_c}}$	Control torque provided by the magnetotorquers on the S/C	$N\ m$
$\underline{\boldsymbol{M}}_d$	Disturbing torques vector	$N\ m$
$\underline{\boldsymbol{M}}_{GG}$	Gravity gradient disturbing torque vector	$N\ m$
$\underline{\boldsymbol{M}}_{SRP}$	Solar radiation pressure disturbing torque vector	$N\ m$
$\underline{\boldsymbol{M}}_{MAG}$	Magnetic field disturbing torques vector	$N\ m$
$\underline{\boldsymbol{M}}_{dr}$	Residual dipole vector	$A\ m^2$
$\boldsymbol{\mu}$	Gravitational planetary constant	km^3/s^2
$\underline{\boldsymbol{n}}$	Angular random walk	rad/s
$\underline{\hat{\boldsymbol{n}}}_{B,i}$	Normal direction to the i-surface	$-$
$\boldsymbol{n_{sun}}$	Mean motion of Earth with respect of Sun	rad/s
$\boldsymbol{N_{surf}}$	Number of surfaces of the S/C	$-$
$\boldsymbol{\Omega}$	RAAN of the orbit	rad
$\boldsymbol{\omega}$	Argument of pericenter of the orbit	rad
$\underline{\boldsymbol{\omega}}_B^{meas}$	Measured angular velocity vector	rad/s
$\underline{\boldsymbol{\omega}}_d$	Desired angular velocity vector	rad/s
$\underline{\boldsymbol{\omega}}_e$	Error angular velocity vector	rad/s
$\underline{\boldsymbol{\omega}}$	Angular velocity vector	rad/s
$\underline{\dot{\boldsymbol{\omega}}}$	Angular acceleration vector	rad
$\boldsymbol{\phi}$	Euler's angle of rotation around z axis	rad
$\dot{\boldsymbol{\phi}}$	Euler's angle angular velocity around z axis	rad/s
$\boldsymbol{\psi}$	Euler's angle of rotation around y axis for 312 and z for 313	rad

Variable	Description	Unit
$\dot{\psi}$	Euler's angle angular velocity around y axis for 312 and z for 313	rad/s
r	Magnitude of the position of the S/C	km
$\underline{r}$	Position of the S/C	km
$\underline{\ddot{r}}$	Double derivative of the position of the S/C	km/s^2
$\underline{r}_N$	Position of the S/C in the inertial frame	km
$\underline{r}_B$	Position of the S/C in the body frame	km
R_E	Earth's radius	km
ρ_d	Diffuse reflection coefficient	$-$
ρ_s	Specular reflection coefficient	$-$
σ_m	Random magnetic measurement error	T
$\underline{\hat{S}}_B$	Direction of the Sun in the body frame	$-$
$\underline{\hat{S}}_N$	Direction of the Sun in the inertial frame	$-$
T_{orb}	Orbital period	s
θ	Euler's angle of rotation around x axis	rad
$\dot{\theta}$	Euler's angle angular velocity around x axis	rad/s
Θ	Angular position of the S/C on the orbit	rad
ξ_m	Inclination of S/C wrt geomagnetic equatorial plane	$\circ$

1 Intoduction

The spacecraft used as a model is a generic 6U CubeSat with two deployable solar arrays considered fixed in the top portion. Its geometric properties can be seen in Table 1.1 while Figure 1.1 shows a representation of the model.

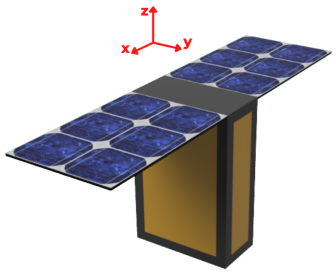

Figure 1.1: CubeSat model

	Size [m]	**Mass [m]**
Main body	0.1 x 0.2 x 0.3	7.98
Solar panel	0.2 x 0.3	0.127
Total		8.4880

Table 1.1: Assignment Data

Due to the presence of the solar panels, the center of mass of whole the spacecraft is 0.8 cm above the one of the main body, while the inertia matrix of the system is:

$$\mathrm{I} = \begin{bmatrix} 0.0988 & 0 & 0 \\ 0 & 0.0810 & 0 \\ 0 & 0 & 0.0590 \end{bmatrix} \quad [\mathrm{kg} \cdot \mathrm{m}^2]$$

The operational orbit chosen for the project is a Sun Synchronous, with $\Omega = \pi \ rad$ specifically set to obtain as much time in solar light as possible. The complete set of Keplerian elements are shown in table 1.2

a [10^4km]	**e [−]**	**i [deg]**	**Ω [rad]**	ω **[rad]**	θ **[rad]**
0.7195	0	98.7	π	1.6	0

Table 1.2: Keplerian Elements of the selected orbit

2 ADCS Architecture

The selected ADCS architecture can be seen in Figure 2.1, and it includes:

- Four sensors: Sun Sensor, Magnetometer, Earth Horizon Sensor and a Gyroscope;
- Two actuators: Magnetic Torquers and Reaction Wheel.

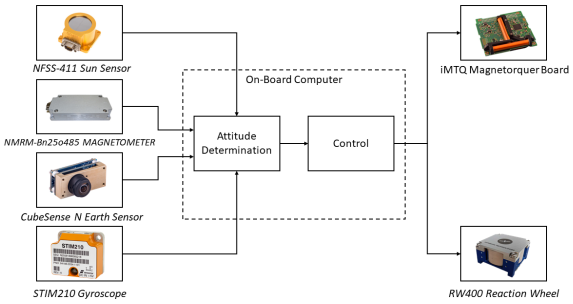

Figure 2.1: ADCS Architecture representation

2.1. Sensors

In order to retrieve the attitude of the spacecraft a Sun sensor, a magnetometer and two Earth sensor are used; moreover to obtain information about the angular velocity, a gyroscope was selected.

2.1.1. Sun Sensor: NFSS-411

Field of view	Accuracy	Mass	Power	Dimensions
140 °	≤ 0.1 °	≤ 5 g	150 mW	34 x 40 x 20 mm

Table 2.1: Sun Sensor datasheet [7]

2.1.2. Magnetometer: NMRM-Bn25o485

Orthogonality	Resolution	Power	Dimensions
± 1 °	< 8 μT	$<$ 750 mW	99 x 43 x 17 mm

Table 2.2: Magnetometer datasheet [6]

2.1.3. Earth Sensor: CubeSense N x 2

Field of view	Accuracy	Mass	Power	Dimensions
180 °	≤ 0.2 °	30 g	100 mW	18 x 42 x 23 mm

Table 2.3: Earth Sensor datasheet [3]

2.1.4. Gyroscope: STIM210

ARW	RRW	Mass	Power	Dimensions
0.15 $°/\sqrt{h}$	± 0.0003 $°/h^{3/2}$	52 g	1.5 W	21.5 x 44.8 x 38.6 mm

Table 2.4: Gyroscope datasheet [8]

2.2. Actuators

To control the spacecraft, a set of four reaction wheels and a magnetotorquer were chosen.

2.2.1. Reaction Wheel: RW400

Total momentum	Maximum torque	Mass	Power	Dimensions
± 15 $mN/m_{/}s$	± 8 mN/m	155 g	1900 mW	50 x 50 x 27 mm

Table 2.5: Reaction wheel datasheet [5]

2.2.2. Magnetotorquer: iMTQ Board

Max Power consumption	Mass	Dimensions
< 1.2 mW	196 g	95.9 x 90.1 x 17 mm

Table 2.6: Magnetotorquer datasheet [5]

3 Model Description

3.1. Orbital Mechanics

The motion of the S/C around Earth is described by the following differential equation:

$$\ddot{\mathbf{r}} = -\frac{\mu}{r^3}\mathbf{r}$$

The position at each time step is computed integrating two times the acceleration and it is expressed in the *Earth-Centered Equatorial Inertial (ECEI)* reference frame.

Inside the model a *Sun Synchronous Orbit (SSO)* is used. This is a near polar orbit whose plane direction is fixed with respect to the Sun. In order to be consistent with the characteristic of the SSO orbit, the J2 perturbation was implemented.

$$\ddot{\mathbf{r}} = -\frac{\mu}{r^3}\mathbf{r} + \mathbf{a}_{J_2}$$

$$\mathbf{a}_{J_2} = \frac{3}{2}\frac{J_2 \mu R_e^2}{r^4}\left[\frac{x}{r}\left(5\frac{z^2}{r^2}-1\right)\hat{\mathbf{i}} + \frac{y}{r}\left(5\frac{z^2}{r^2}-1\right)\hat{\jmath} + \frac{z}{r}\left(5\frac{z^2}{r^2}-3\right)\hat{\mathbf{k}}\right]$$

3.2. Attitude dynamics and kinematics

Using the Euler's equations for rigid body motion, the behaviour of the spacecraft in orbit can be obtained. Euler equation has the following form:

$$\mathbf{I}\dot{\underline{\omega}} = \mathbf{I}\underline{\omega} \times \underline{\omega} + \underline{M} \tag{3.1}$$

where $\mathbf{I}$ is the inertia matrix of the satellite, $\underline{\omega}$ is the angular velocity of the spacecraft in the body frame and $\underline{M}$ represents the sum of the torques coming from disturbing forces in the environment and from the actuators on board, used to control the motion of the spacecraft.

Equation 3.1 can be expressed in the expanded form more suitable for implementing into the *Simulink*:

$$\begin{cases} \dot{\omega}_x = \frac{I_y - I_z}{I_x}\omega_y\omega_z + \frac{M_x}{I_x} \\ \dot{\omega}_y = \frac{I_z - I_x}{I_y}\omega_x\omega_z + \frac{M_y}{I_y} \\ \dot{\omega}_z = \frac{I_x - I_y}{I_z}\omega_x\omega_y + \frac{M_z}{I_z} \end{cases} \tag{3.2}$$

Integrating Equation 3.2, the time history of the angular velocities can be obtained. Furthermore, from angular velocities using kinematic relationships, the orientation of the spacecraft's body frame with respect to some other reference frame can be obtained.

For this project, Euler angles ϕ, θ and ψ are used to describe the orientation of the spacecraft's body frame with respect to the inertial reference frame. Twelve distinct sequences of Euler angles exists and the one chosen for the present project is the sequence 312. The equations which need to be integrated in order to obtain time history of the angles are reported in the following expression:

$$\text{sequence } 312 \begin{cases} \dot{\phi} = \frac{(\omega_w \cos\psi - \omega_u \sin\psi)}{\cos\vartheta} \\ \dot{\vartheta} = \omega_u \cos\psi + \omega_w \sin\psi \\ \dot{\psi} = \omega_v - (\omega_w \cos\psi - \omega_u \sin\psi)\frac{\sin\vartheta}{\cos\vartheta} \end{cases} \tag{3.3}$$

After each angle is obtained in every time instant, the complete direction cosine matrix $\mathbf{A_{312}}\ (\phi, \theta, \psi)$ can be calculated with the following expression:

$$\mathbf{A_{312}} = \begin{bmatrix} \cos\psi\cos\phi - \sin\psi\sin\phi\sin\vartheta & \cos\psi\sin\phi + \sin\psi\cos\phi\sin\vartheta & -\sin\psi\cos\vartheta \\ -\sin\phi\cos\vartheta & \cos\phi\cos\vartheta & \sin\vartheta \\ \sin\psi\cos\phi + \cos\psi\sin\phi\sin\vartheta & \sin\psi\sin\phi - \cos\psi\cos\phi\sin\vartheta & \cos\vartheta\cos\psi \end{bmatrix}$$

When using Euler angles to represent the kinematics of the spacecraft, particular care must be taken in order to avoid singularities. This is very important point and a drawback of using this way to represent the attitude of the spacecraft. Depending on the set of Euler angles used, this condition is different. For the sequence 312 the singularity arises when $\theta = (2n+1)\pi/2$. In order to avoid singularity, a second sequence of Euler angles is used in combination with the one mentioned above. This is the sequence 313 and the expression needed to obtain the time history of the angles has the following form:

$$\text{sequence } 313 \begin{cases} \dot{\phi} = \frac{(\omega_u \sin\psi + \omega_v \cos\psi)}{\sin\vartheta} \\ \dot{\vartheta} = \omega_u \cos\psi - \omega_v \sin\psi \\ \dot{\psi} = \omega_w - (\omega_u \sin\psi + \omega_v \cos\psi)\frac{\cos\vartheta}{\sin\vartheta} \end{cases} \tag{3.4}$$

After each angle is obtained in every time instant, the complete direction cosine matrix $\mathbf{A_{313}}(\phi, \theta, \psi)$ can be calculated with the following expression:

$$\mathbf{A_{313}} = \begin{bmatrix} \cos\psi\cos\phi - \sin\psi\sin\phi\cos\vartheta & \cos\psi\sin\phi + \sin\psi\cos\phi\cos\vartheta & \sin\psi\sin\vartheta \\ -\sin\psi\cos\phi - \cos\psi\sin\phi\cos\vartheta & -\sin\psi\sin\phi + \cos\psi\cos\phi\cos\vartheta & \cos\psi\sin\vartheta \\ \sin\phi\sin\vartheta & -\cos\phi\sin\vartheta & \cos\vartheta \end{bmatrix}$$

Still, problem with singularity is not solved due to the fact that for sequence 313 singularity occurs when $\theta = n\pi$. In order to completely avoid reaching the singularity with two sequences, algorithm shown in Figure 3.1 is implemented inside the *Simulink*. This algorithm is designed in order to switch between the two sequences whenever θ for the sequence 312 falls into a given range, which can be seen in Figure 3.1.

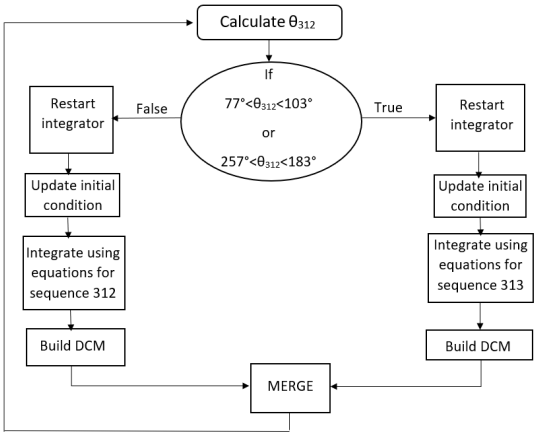

Figure 3.1: Blockscheme of the singularity avoidance algorithm

3.3. Disturbance Torques

The S/C along its orbit is subjected to disturbance torques, generated by external environmental factors, that affect its dynamics. The disturbances considered inside the model are the gravity gradient torque, the solar radiation pressure (SRP) torque and the Earth's magnetic field torque. The total disturbing net torque acting on the S/C is computed as the summation of these contributions:

$$\underline{M}_d = \underline{M}_{GG} + \underline{M}_{SRP} + \underline{M}_{MAG}$$

The disturbance torque due to atmospheric drag is not considered since it is negligible for orbit altitudes higher than 700 km.

3.3.1. Gravity Gradient

The gravity gradient torque is generated due to the different gravitational forces acting on the S/C parts, depending on their position with respect to Earth.

The torque is computed as follows:

$$\mathbf{M_{GG}} = \frac{3Gm_{\text{Earth}}}{r_{s/c}^3} \begin{bmatrix} (Iz - Iy)c_2c_3 \\ (Ix - Iz)c_1c_3 \\ (Iy - Ix)c_1c_2 \end{bmatrix}$$

where $r_{S/C}$ is the magnitude of the S/C position and $c1, c2$ and $c3$ are:

$$\begin{bmatrix} c_1 \\ c_2 \\ c_3 \end{bmatrix} = \mathbf{A_{B/L}} \begin{bmatrix} 1 \\ 0 \\ 0 \end{bmatrix}$$

The matrix $\mathbf{A_{B/L}}$ is the matrix of the relative attitude between the rotating body frame (B) and the local vertical local horizon (LVLH) frame.

$$\mathbf{A_{B/L}} = \mathbf{A_{B/N}} \mathbf{A^T_{L/N}}$$

where $\mathbf{A_{L/N}}$ depends on orbit inclination and position.

$$\mathbf{A_{L/N}} = \begin{bmatrix} \cos\theta & \sin\theta & 0 \\ -\sin\theta & \cos\theta & 0 \\ 0 & 0 & 1 \end{bmatrix} \begin{bmatrix} 1 & 0 & 0 \\ 0 & \cos i & \sin i \\ 0 & -\sin i & \cos i \end{bmatrix}$$

3.3.2. Solar Radiation Pressure

In order to compute the torques of the SRP, it is necessary to know the direction of Sun with respect to the rotating body frame $\underline{\hat{S}}_B$:

$$\underline{\hat{S}}_B = \mathbf{A_{B/N}} \underline{\hat{S}}_N = \mathbf{A_{B/N}} \begin{Bmatrix} \cos\left(n_{\text{Sun}}\, t\right) \\ \sin\left(n_{\text{Sun}}\, t\right) \cos\left(23.45^\circ\right) \\ \sin\left(n_{\text{Sun}}\, t\right) \sin\left(23.45^\circ\right) \end{Bmatrix}$$

The direction of Sun with respect of the inertial frame $\underline{\hat{S}}_N$ depends on the mean motion, $n = \frac{2\pi}{1year}$ and the obliquity angle, $\epsilon = 23.45^\circ$. The Sun's direction with respect to the S/C, can be approximated by the Sun's direction with respect to Earth, since the distance between Earth and Sun is much greater than the distance between Earth and the S/C.

At an altitude of approximately 800 km from Earth's surface, the main sources of radiation illuminating S/C surfaces are:

Direct solar radiation	**Radiation reflected by Earth**	**Earth radiation**
1358 W/m^2	540 W/m^2	130.2 W/m^2

The orientation of each outer panel of the S/C is defined through perpendicular vectors to surfaces. In particular with the n_i vectors with $i = 1$ to 6, the surfaces of the main body are described whereas with the n_i vectors with $i = 7$ to 10 the solar panel surfaces are characterized.

Moreover, each surface is associated with a given specular and diffuse reflection coefficients (ρ_s, ρ_d): for solar panels $\rho_s = 0.1$, for the main body $\rho_s = 0.5$ and a diffuse coefficient $\rho_d = 0.1$ for all the surfaces.

With a total value of power per unit of surface, given by the summation of the radiation contributions previously described, equal to $F_e = 2028.2\ \mathrm{W/m^2}$, the forces due to SRP are computed:

$$\underline{F}_i = -\frac{F_e}{c} A_i \left(\hat{\underline{S}}_B \cdot \hat{\underline{n}}_{B,i}\right) \left\{ (1 - \rho_{s,i})\, \hat{\underline{S}}_B + \left[2\rho_{s,i} \left(\hat{\underline{S}}_B \cdot \hat{\underline{n}}_{B,i}\right) + \frac{2}{3}\rho_{d,i} \right] \hat{\underline{n}}_{B,i} \right\}$$

where i=1, ..., N_{surf}.

If $(\underline{S}_B \cdot \hat{\underline{n}}_{B,i}) > 0$ the torque $\underline{M}_{SRP}$ is computed as in the following equation, otherwise the torque is 0 because the surface is not exposed to the Sun.

$$\underline{M}_{SRP} = \sum_{i=1}^{N_{\mathrm{surf}}} \underline{r}_i \times \underline{F}_i$$

3.3.3. Earth's Magnetic Field

The model of Earth's magnetic field can be described for simplicity with a dipole model, so it can be computed as:

$$\underline{b}_N = \frac{R_E^3 H_0}{\|\underline{r}\|^3} [3(\hat{\underline{m}} \cdot \hat{\underline{r}})\hat{\underline{r}} - \hat{\underline{m}}] \tag{3.5}$$

where R_E is Earth's radius, $\hat{\underline{r}}$ is the unit vector of Earth's direction in the inertial reference frame and $\hat{\underline{m}}$ is the magnetic dipole direction, inclined to 11.5° with respect to Earth's rotation axis, computed as:

$$\hat{\underline{m}} = \begin{bmatrix} \sin 11.5^\circ \cos \omega_E t \\ \sin 11.5^\circ \sin \omega_E t \\ \cos 11.5^\circ \end{bmatrix}$$

In equation (3.5), H_0 is evaluated as:

$$H_0 = \sqrt{\left(g_0^1\right)^2 + \left(g_1^1\right)^2 + \left(h_1^1\right)^2}$$

and it is related to the Gaussian coefficients g_n^m and h_n^m calculated experimentally and catalogued by the International Geomagnetic Reference Field (IGRF). The coefficients change over time, due to the change in the magnetic field, and are updated every 5 years. The ones used in the model are referred to IGRF 2000 standard values.

The magnetic torque is computed as:

$$\underline{M}_{MAG} = \underline{M_{dr}} \times \mathbf{A_{B/N}} \underline{b}_N = \underline{M_{dr}} \times \underline{b}_B$$

where $\underline{M}$ is the residual dipole of the satellite due to on-board currents:

$$\underline{M_{dr}} = \{0.1, 0.5, 0.1\}^T A/m^2$$

3.4. Sensors

In this section the model used to implement the selected sensors is analyzed. Up to this point all the signals were considered continuous; however, since the sensors reflect the measurement of the real World, a Zero-Order-Hold block was used to discretize the data.

3.4.1. Magnetometer

To model magnetic field sensor, the non-orthogonality error that may arise due to the fact that the sensor's axis are not exactly orthogonal to each other must be taken into account. This is usually obtained from calibration but for the this purpose it is modeled with a non-orthogonal matrix, $\mathbf{A}_\epsilon$ where the off-diagonal terms are selected to be $< \pm 1°$ according to the datasheet, and considered to be constant, for the whole mission:

$$\mathbf{A}_\epsilon = \begin{bmatrix} 1 & \alpha_{zx} & \alpha_{yx} \\ \alpha_{zy} & 1 & \alpha_{xy} \\ \alpha_{yz} & \alpha_{xz} & 1 \end{bmatrix}$$

Another error that needs to be taken into account is the one arising from the error in the magnitude (non perfect measurement of the value of the magnetic field). This is modelled as a random error with variance equal to the noise density of the sensor given in the datasheet and a mean value of zero which is added to the each component of the true magnetic field. The complete model of the sensor is represented in the following way:

$$\underline{b}_B = \mathbf{A}_\epsilon \mathbf{A_{B/N}} \underline{b}_N + \sigma_m$$

3.4.2. Gyroscope

The angular velocity is computed using the following equation:

$$\underline{\omega_B}^{meas} = \underline{\omega_B} + \underline{n} + \underline{b}$$

Where $\underline{\omega_B}$ is the real angular velocity obtained in the dynamics and $\underline{n}$, $\underline{b}$ are two sources

of disturbances. In fact this family of sensor is typically affected by two white Gaussian noise with zero mean:

- ARW: is the angular random walk, due to thermo mechanical noise of the system and given by $\underline{n} = \sigma_n \underline{\zeta}_n$
- RRW: is the rate random walk, due to electronic noise and given by $\dot{\underline{b}} = \sigma_b \underline{\zeta}_b$

Due to high level of noise a low-pass filter was used to reduce oscillation in the signal.

3.4.3. Sun Sensor and Earth Horizon Sensor

Sun sensor and Earth Horizon sensor measure respectively the direction of Sun and the position's direction of S/C in the body frame. Both sensors are modeled implementing an error matrix, in order to simulate the measurements error of the direction vectors measured. The error matrix $\mathbf{A}_\epsilon$ is the following:

$$\mathbf{A}_\epsilon = \begin{bmatrix} 1 & -\alpha_z & \alpha_y \\ \alpha_z & 1 & -\alpha_x \\ -\alpha_y & \alpha_x & 1 \end{bmatrix}$$

where α_x, α_y, α_z are computed as random numbers using the variance of the accuracy of each sensor, tabulated in tables 2.1 and 2.4. Moreover, the random numbers generated are filtered by a low pass filter to moderate the oscillations. The measured direction of Sun in the body frame is:

$$\underline{\hat{S}}_B = \mathbf{A}_\epsilon \mathbf{A}_{\mathbf{B/N}} \underline{\hat{S}_N}$$

The measured direction of S/C position in the body frame is:

$$\underline{\hat{r}}_B = \mathbf{A}_\epsilon \mathbf{A}_{\mathbf{B/N}} \underline{\hat{r}_N}$$

3.5. Actuators

3.5.1. Magnetotorquers

Torque exerted on the spacecraft by the magnetic torquer in the presence of the external magnetic field when current is applied through ferromagnetic core is modeled in the following way:

$$\underline{M}_c = \underline{m} \times \underline{b}_B$$

where $\underline{m}$ is the commanded magnetic dipole moment generated by the torquers, $\underline{b}_B$ is the local magnetic field expressed in the body-frame coordinates.

Of course, due to the limitations of the magnetic dipoles, for simulation purposes, the maximum magnetic dipole is limited to $1Am^2$.

3.5.2. Reaction Wheels

Reaction wheels are used as a second actuator on the cubesat. In particular four reaction wheels are used, one aligned with each principal inertia axis and the fourth one on the diagonal. Using four instead of three allows for redundancy in case of malfunctions. The reaction wheels can be modeled by Equation 3.6, that gives the torque that needs to be applied to the reaction wheel:

$$\dot{\underline{h}}_r = -\mathbf{A}^* \left(\underline{M}_c + \underline{\omega} \times \mathbf{A}\underline{h}_r\right) \tag{3.6}$$

where $\mathbf{A}^*$ is the pseudoinverse of matrix $\mathbf{A}$, $\underline{M}_c$ is the control torque and $\underline{\omega}$ the angular velocity of the reaction wheel.

Matrices $\mathbf{A}$ and $\mathbf{A}^*$ are shown in equations 3.7 and 3.8 respectively.

$$\mathbf{A} = \begin{bmatrix} 1 & 0 & 0 & 1/\sqrt{3} \\ 0 & 1 & 0 & 1/\sqrt{3} \\ 0 & 0 & 1 & 1/\sqrt{3} \end{bmatrix} \tag{3.7}$$

$$\mathbf{A}^* = \begin{bmatrix} 5/6 & -1/6 & -1/6 \\ -1/6 & 5/6 & -1/6 \\ -1/6 & -1/6 & 5/6 \\ 1/2\sqrt{3} & 1/2\sqrt{3} & 1/2\sqrt{3} \end{bmatrix} \tag{3.8}$$

Once torque that needs to be applied to each reaction wheel is calculated, influence of reaction wheel on motion of the spacecraft can be seen in the following equation:

$$\mathbf{I}\dot{\underline{\omega}} + \underline{\omega} \times \mathbf{I}\underline{\omega} + \underline{\omega} \times \mathbf{A}\underline{h}_r + \mathbf{A}\dot{\underline{h}}_r = \underline{M}_d$$

4 Attitude determination and control algorithms

4.1. Attitude determination

For the attitude determination of the satellite, a statistical approach is used. In particular the algorithm developed gives the solution to what is known as the Wabha's problem. This results from minimizing the following:

$$J(\mathbf{A}) = \frac{1}{2}\sum_{i=1}^{N} \alpha_i \left| s_{Bi} - \mathbf{A_{B/N}} v_{Ni} \right|^2$$

where N is the number of sensors, α_i shows the weight each sensor has, s_{Bi} is a unit vector in the body frame and v_{Ni} is a unit vector in the inertial frame.

Minimizing the above equation is equivalent to maximizing the function below:

$$\tilde{J}(\mathbf{A}) = \sum_{i=1}^{N} \alpha_i s_{Bi}^T \mathbf{A_{B/N}} v_{Ni} = \mathrm{tr}\left(\mathbf{A_{B/N}} \mathbf{B}^T\right)$$

where $\mathbf{B} = \sum_{i=1}^{N} \alpha_i s_{Bi} v_{Ni}^T$

Using singular value decomposition $\mathbf{B}$ can be rewritten as shown below

$$\mathbf{B} = \mathbf{U}\Sigma^T\mathbf{V^T} = \mathbf{U}\,\mathrm{diag}\begin{bmatrix} \Sigma_{11} & \Sigma_{22} & \Sigma_{33} \end{bmatrix}^T \mathbf{V^T}$$

where $\mathbf{U}$ and $\mathbf{V}$ are unitary orthogonal matrices, $\mathbf{U}$ representing the eigevectors of matrices $\mathbf{BB^T}$ and $\mathbf{V}$ of matrices $\mathbf{B^TB}$. The values of Σ are the square roots of the eigenvalues of matrix $\mathbf{B^TB}$ or of matrix $\mathbf{BB^T}$.

Finally $\mathbf{A_{B/N}}$ can be computed as

$$\mathbf{A_{B/N}} = \mathbf{U}M\mathbf{V^T}$$

where $M = \mathrm{diag}\begin{bmatrix} 1 & 1 & (\det \mathbf{U})(\det \mathbf{V}) \end{bmatrix}$

Since attitude determination cannot be performed if measurements are parallel, analysis is performed in order to ensure that during each phase of the mission, appropriate set of

sensors is fed into the attitude determination block. Furthermore, in order to be capable to obtain measurements, both Sun sensor and Earth horizon sensor must have Sun and Earth in the field of view. Therefore, the following sensors are used in different mission phases to obtain the attitude of the spacecraft:

1. Detumbling: integrating kinematics with the angular velocities obtained with gyroscope
2. Inertial pointing and slew maneuver: sun sensor + Earth horizon sensor up to 1000 seconds and sun sensor + magnetometer after 1000 seconds,
3. Tracking: Earth horizon sensor + magnetometer.

Results of this analysis are reported in the subsequent chapter.

4.2. Detumbling

In this phase of the mission, the spacecraft's angular velocity should be brought as close to zero as possible. The spacecraft is considered detumbled, when it follows the magnetic field around the Earth. This means, that at an altitude of $800km$, the angular velocity of the spacecraft, must be below $0.1°/s$ [1]. Attitude control system which is proposed to detumble a spacecraft is based on using three magnetotorquers as an actuators. This type of system is underactuated since as one of the magnetic torquers can be aligned with the external magnetic field direction and therefore produce no torque at this moment. However, during detumbling the spacecraft is rotating, so the direction of magnetic field in the body frame is always changing. The control of the spacecraft is achieved by simply commanding a magnetic dipole moment expressed in the following way [4]:

$$\underline{m} = \frac{k}{\|\underline{b}_B\|}\underline{\omega} \times \underline{b}$$

where $\underline{b} = \frac{\underline{b}_B}{\|\underline{b}_B\|}$, $\underline{\omega}$ represents angular velocity of the spacecraft in the body frame and k represents the positive scalar gain.

It follows that actual torque applied to the spacecraft has the following expression:

$$\underline{M_c} = \underline{m} \times \underline{B}$$

where M_c denotes real control torque applied to the spacecraft.

The value of the positive scalar gain k can be obtained in the following way [4]:

$$k = \frac{4\pi}{T_{orb}}(1 + sin(\xi_m))J_m$$

where T_{orb} is the orbital period in seconds, ξ_m is the inclination of the spacecraft relative to the geomagnetic equatorial plane and J_m is the minimum principal moment of inertia. Therefore, in this case $k = 2.3686 \times 10^{-4}$.

4.3. Sun pointing and slew maneuver

This phase of the mission consists of pointing z-axis of the spacecraft's body frame to the sun direction for 1000 seconds in order to have solar panels completely illuminated for charging the electrical equipment and then performing the slew maneuver to a different, arbitrarily chosen inertial position. Due to the fact that sun direction is changing very slowly and taking into account the time of the simulation, it can be considered fixed. Furthermore, y-axis of the body frame is aligned with the y-axis of the inertial frame, while x-axis of the body frame is aligned with -z-axis of the inertial frame for the secondary pointing requirement (to have Earth in the field of view of the Earth horizon sensor). This means that the initial desired attitude orientation expressed in terms of Euler angles is $\underline{\alpha}_d = [0, 0, 90]^\circ$. The requirement for attitude control system in this phase is that the pointing error, ϵ_r, is less than 5°, and the result is considered stable when the angular rate does not differ more than $0.001^\circ/s$, which is ideal for most space missions [2]. In order to achieve the desired attitude orientation, four reaction wheels are used as actuators, while three magnetotorquers are used for desaturation of the reaction wheels. This is done because analyzing the behaviour of magnetic field of the Earth, some of the components become zero during simulation, which would lead to singular condition. Taking this into consideration, the following non linear control law is selected:

$$\underline{M_c} = -k_1 \underline{\omega} - k_2 (\mathbf{A}_e^T - \mathbf{A}_e)^V \tag{4.1}$$

where, M_c is again the calculated ideal control torque, k_1 and k_2 are the positive scalar gains, $(\mathbf{A}_e^T - \mathbf{A}_e)^V = [\mathbf{A}_{e23} - \mathbf{A}_{e32}, \mathbf{A}_{e31} - \mathbf{A}_{e13}, \mathbf{A}_{e12} - \mathbf{A}_{e21}]^T$ and $\mathbf{A_e} = \mathbf{A}\mathbf{A_d^T}$, where $\mathbf{A}$ is the instantaneous orientation of the spacecraft and $\mathbf{A_d}$ is the desired one. The positive scalar gains for the case of sun pointing are obtained by trial and error procedure and they are $k_1 = 9 \times 10^{-3}$ and $k_2 = 3 \times 10^{-4}$.

After 1000 seconds of sun pointing, the spacecraft shall perform slew maneuver where the desired final orientation expressed in term of Euler angles is $\underline{\alpha}_d = [35, 45, 30]^\circ$. Since slew maneuver can be considered as rest to rest maneuver, non linear control law expressed in Equation 4.1 can be used, and also the same actuator setup is considered. For this phase of the mission, the pointing error must be less than 1° and the angular rate must be less than than $0.001^\circ/s$. In the case of the slew maneuver, the positive scalar gains are selected to be $k_1 = 9 \times 10^{-3}$ and $k_2 = 3 \times 10^{-4}$, which are again obtained by trial and error procedure.

4.4. Target tracking

In this phase of the mission, the spacecraft shall track a moving target, which is selected to be Local Vertical Local Horizontal reference frame (LVLH frame), meaning that the desired attitude matrix is $\mathbf{A_d} = \mathbf{A_{L/N}}$. In particular requirement for attitude control is to have pointing error between x-axis of the body frame and x-axis of the LVLH frame less than 1.5°. Furthermore, the desired angular velocity must match the one of the LVLH frame, $\underline{\omega_d} = [0, 0, n]^T rad/s$, where n is the mean orbital velocity of the spacecraft. In order to achieve the desired attitude orientation, like for inertial pointing and slew maneuvers, four reaction wheels are used as actuators, while three magnetotorquers are used for desaturation of the reaction wheels. In order to satisfy the previously mentioned requirements, the following non linear control law is selected to calculate the desired torque:

$$\underline{M_c} = -k_1\underline{\omega_e} - k_2(\mathbf{A_e}^T - \mathbf{A_e})^V + \underline{\omega} \times \mathbf{I}\underline{\omega}$$

where $\underline{\omega_e} = \underline{\omega} - \underline{\omega_d}$ represents error angular velocity and $\mathbf{I}$ represents principal inertia matrix of the spacecraft. Again, gains k_1 and k_2 are obtained by trial and error procedure and they are $k_1 = 9 \times 10^{-3}$, $k_2 = 3 \times 10^{-4}$.

5 | Results

5.1. Detumbling

In this part of the mission, initial conditions after releasing the spacecraft from the launcher are selected to be $\underline{\omega}_0 = [5.72, 11.45, 8.59]^\circ/s$ and $\underline{\alpha}_0 = [0, 0, 0]^\circ$. Motion of the spacecraft is simulated for 3000 seconds. In Figure 5.1a it can be seen that angular velocities are reducing and that after approximately 2000 seconds, the requirement of $0.1^\circ/s$ is met. Since during this phase the spacecraft is tumbling and the field of view of Earth and sun sensor is changing all the time, the attitude of the spacecraft is calculated by integrating the kinematic relationships given with Equation 3.3 and Equation 3.4, where angular velocities coming from gyroscope are used.

As it could be seen in Figure 5.1 after 2500 seconds RW are used to let the S/C point the direction of the Sun, to prepare it for the next phase of the mission. This discussion is represented in Figure 5.1b.

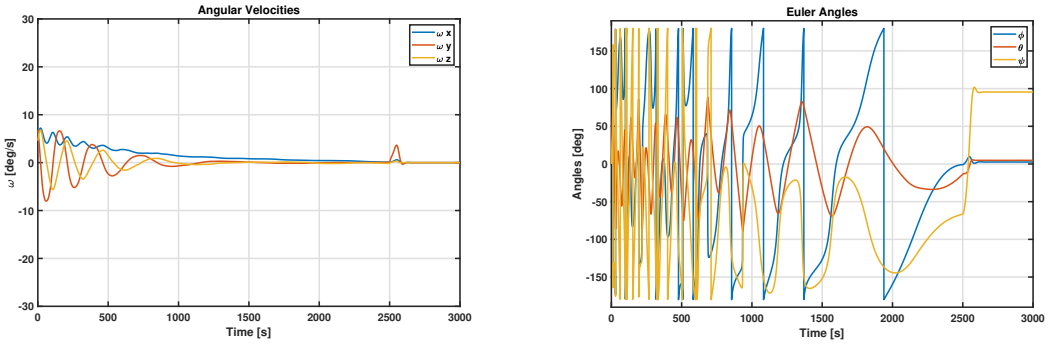

(a) Angular velocity evolution.

(b) Evolution of the Euler angles.

Figure 5.1: Dynamics and kinematics of the spacecraft during the detumbling phase.

During the detumbling phase, only magnetotorquers are used, therefore the commanded dipole moment (with saturation applied) and real torque applied to the sapcecraft are reported in Figure 5.2. In Figure 5.2 it can be seen control torque produced by the reaction wheels in order to prepare spacecraft for future phase of the mission (sun pointing), but for the case of the detumbling it can be neglected.

5.2. Sun pointing and slew maneuver

The initial conditions during this phase of the mission are selected to be $\underline{\omega}_0 = [0, 0, 0]^\circ/s$ and $\underline{\alpha}_0 = [0, 0, 90]^\circ$. The motion of the spacecraft is simulated for 3000 seconds. In Figure

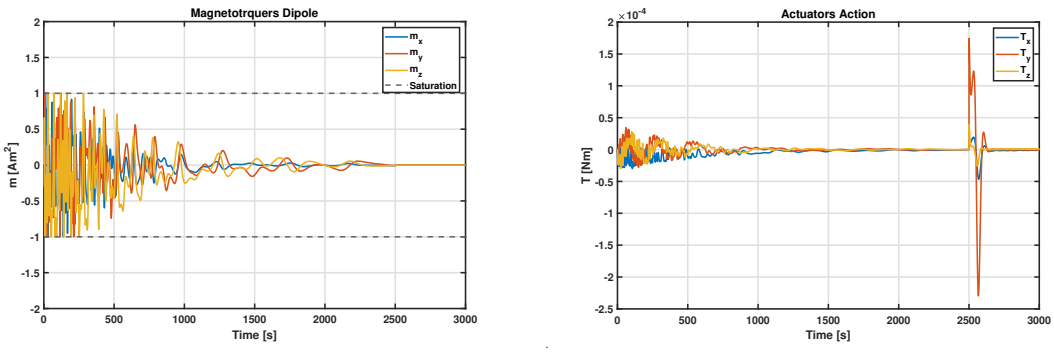

(a) Commanded dipole moment.

(b) Real torque applied to the spacecraft.

Figure 5.2: Behaviour of the actuators during the detumbling phase.

5.3, the time history of angular velocities and Euler's angles is represented. It can be seen that angular velocities requirement are met, since angular velocities are oscillating around $0.001°/s$ apart from the moment when slew maneuver is performed. Furthermore, in Figure 5.3 it can be seen that Euler angles have correct behaviour, meaning that required attitude is achieved.

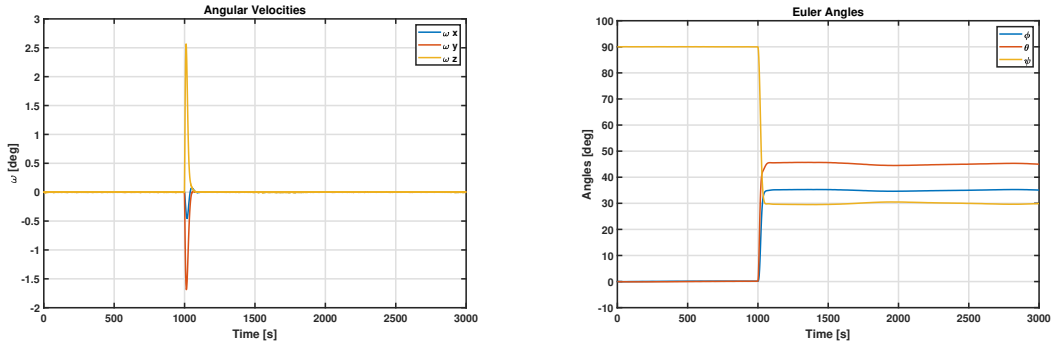

(a) Angular velocity evolution.

(b) Evolution of the Euler angles.

Figure 5.3: Dynamics and kinematics of the spacecraft.

Furthermore, Figure 5.4 shows the pointing error during this phase of the mission. It can be seen that the requirement of pointing error less than 5° for sun pointing is achieved. Also after performing the slew maneuver at 1000 seconds, pointing error becomes less than the required one, 0.5°, meaning that attitude control system is capable of successfully controlling the spacecraft.

As mentioned in previous chapters, during this phase of the mission two combination of two sensors are used. Proof for that can be seen in Figure 5.6a calculating norm of the cross product between two sensors, where due to the better orthogonality properties between measurements, after performing slew maneuver on-board computer is using sun sensor and magnetometer in order to obtain orientation of the spacecraft, while in the

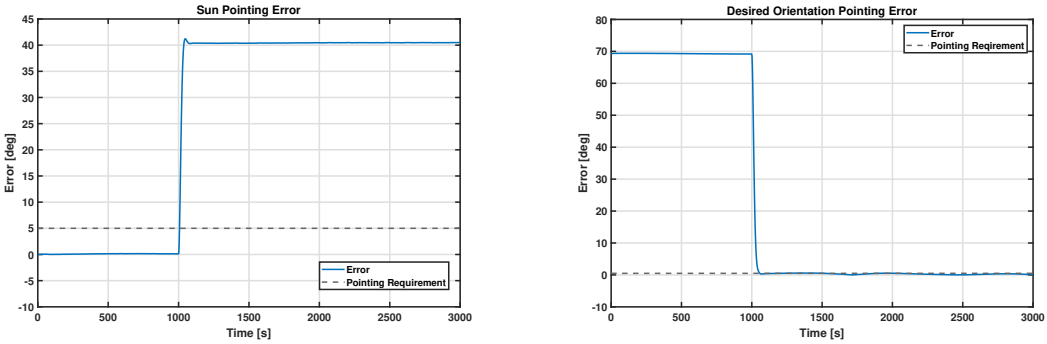

(a) Sun pointing error. (b) Inertial pointing error.

Figure 5.4: Pointing error.

initial phase of the mission, during the sun pointing, Earth horizon and sun sensor gives better attitude estimation. For this reason two Earth horizon sensors must be used, in order to have Earth in the field of view of the sensor. It is also interesting to see that during the entire simulation, the reaction wheels are not saturated. This is evident by looking at Figure 5.6b.

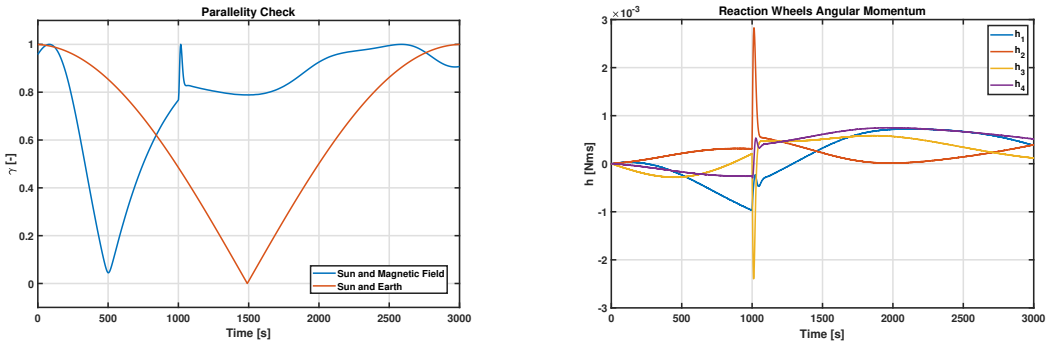

(a) Parallelity check. (b) Angular momentum of the reaction wheels.

Figure 5.5: Parallelity check and angular momentum of the reaction wheels.

5.2.1. Uncontrolled pointing

After 3000 seconds pointing control law and also reaction wheels are switched off in order to see the difference between controlled and uncontrolled case. This can be seen in Figure 5.6. As can be noticed angular velocities starts diverging and pointing error starts to increase due to environment disturbances, which is expected. Therefore, spacecraft is not able to achieve the imposed requirement in uncontrolled case.

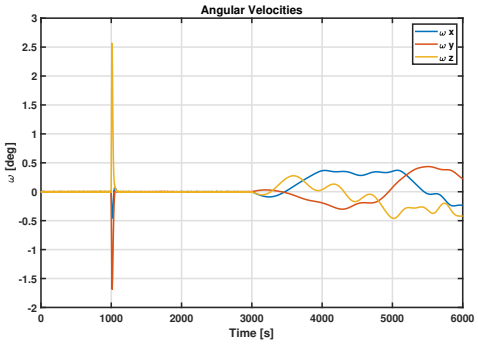

(a) Evolution of the angular velocities.

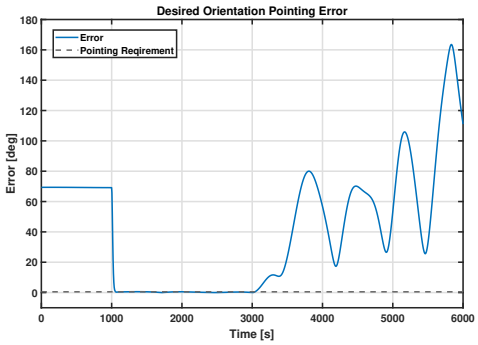

(b) Pointing error.

Figure 5.6: Switch between controlled and uncontrolled spacecraft.

5.3. Tracking

Initial conditions during this phase of the mission are selected to be $\underline{\omega}_0 = [0, 0, 0]^\circ/s$ and $\underline{\alpha}_0 = [35, 45, 30]^\circ$. Motion of the spacecraft is simulated for 3000 seconds. In Figure 5.7 angular velocities as well as orientation of the spacecraft's body frame with respect to the LVLH frame represented in term of Euler angles can be seen. From Figure, it can be noticed that angular velocity of the spacecraft along z-axis is in the close proximity to the mean orbital motion of the spacecraft. Furthermore, Euler angles are close to zero, which is expected since they are computed with respect to LVLH frame.

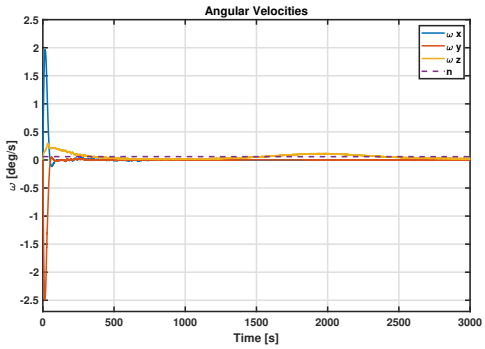

(a) Evolution of the angular velocities.

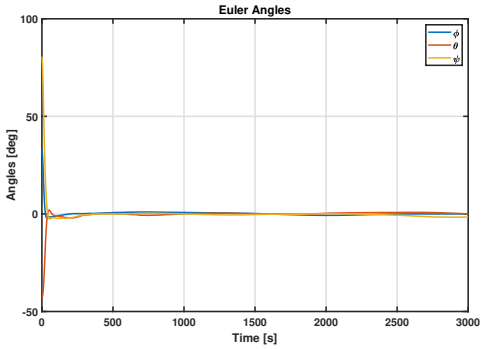

(b) Evolution of the Euler angles.

Figure 5.7: Attitude dynamics and kinematics during the tracking phase.

Pointing error with respect to the ideal nadir pointing is represented in Figure 5.8a. It can be seen that pointing error is in the desired range apart from the final part of the simulation time (2500 seconds). This is expected since in this part of the orbit Earth sensor and magnetometer measurements become more parallel, therefore there will be more error in attitude estimation, which is reflected to the overreaction of the control law which causes slight deviation in the real orientation of the spacecraft (Figure 5.8b).

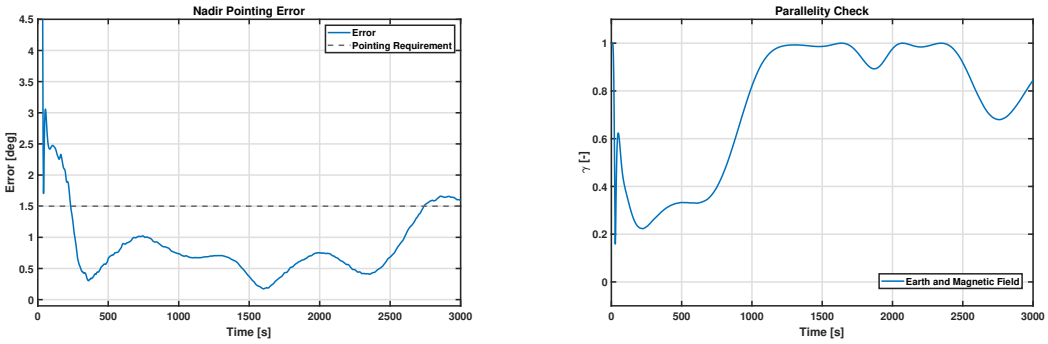

(a) Nadir pointing error.

(b) Parallelity check.

Figure 5.8: Nadir pointing error and paralleilty check for sensors.

For this phase of the mission sun sensor cannot be used because sun is not in the field of the view of the sensor which can be seen in Figure 5.9a. Of course sun sensor can be added but since requirement is also achieved with less expensive sensor there is no need to introduce additional cost by putting one more sun sensor since pointing requirement is achieved. Finally, in Figure 5.9b it can be seen that reaction wheels do not get saturated during this phase of the mission.

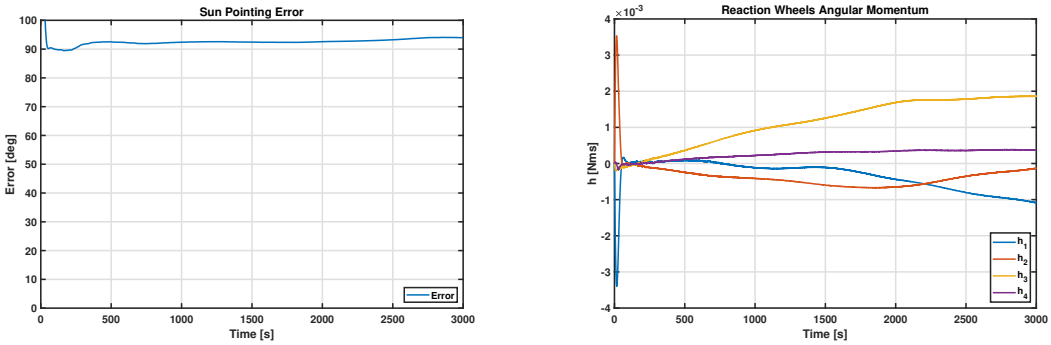

(a) Sun pointing error.

(b) Angular momentum of the reaction wheels.

Figure 5.9: Checking sun direction and angular momentum saturation.

Bibliography

[1] O. A. Bo, G. Claus, H. K. Rasmus, N. Claus, K. S. Kresten, and T. Dan. Attitude control system for aausat-ii. 2005.

[2] X. Cao, C. Yue, M. Liu, and B. Wu. Time efficient spacecraft maneuver using constrained torque distribution. *Acta Astronautica*, 123, 03 2016. doi: 10.1016/j.actaastro.2016.03.026.

[3] CubeSpace. Cubesense n earth sensor datasheet. URL `https://www.cubespace.co.za/products/adcs-components/cubesense/`.

[4] J. L. C. F.Landis Markley. *Fundamentals of Spacecraft Attitude Determination and Control*. Springer, 2014. ISBN 978-1-4939-0802-8.

[5] Isispace. imtq magnetorquer board datasheet. URL `https://www.isispace.nl/product/isis-magnetorquer-board/`.

[6] NewSpace-Systems. Nmrm-bn25o485 magnetometer datasheet, . URL `https://www.newspacesystems.com/wp-content/uploads/2020/10/NewSpace-Magnetometer_2020_10a.pdf`.

[7] NewSpace-Systems. Nfss-411 sun sensor datasheet, . URL `https://www.newspacesystems.com/wp-content/uploads/2021/10/NewSpace-Sun-Sensor_20211018_2020-10e.pdf`.

[8] Sensor. Stim210 gyroscope datasheet. URL `https://d29ykr7lqkqqrr.cloudfront.net/media/vxudyo3g/ts1545-r20-datasheet-stim210.pdf`.